City Research Online

City, University of London Institutional Repository

Citation: Reyes-Aldasoro, C. C. & Bhalerao, A. (2003). Volumetric texture description and discriminant feature selection for MRI. Information Processing in Medical Imaging, 2732, pp. 282-293. doi: 10.1007/978-3-540-45087-0_24

This is the accepted version of the paper.

This version of the publication may differ from the final published version.

Permanent repository link: https://openaccess.city.ac.uk/id/eprint/4315/

Link to published version: https://doi.org/10.1007/978-3-540-45087-0_24

Copyright: City Research Online aims to make research outputs of City, University of London available to a wider audience. Copyright and Moral Rights remain with the author(s) and/or copyright holders. URLs from City Research Online may be freely distributed and linked to.

Reuse: Copies of full items can be used for personal research or study, educational, or not-for-profit purposes without prior permission or charge. Provided that the authors, title and full bibliographic details are credited, a hyperlink and/or URL is given for the original metadata page and the content is not changed in any way.

City Research Online: http://openaccess.city.ac.uk/ publications@city.ac.uk

Volumetric Texture Description and Discriminant Feature Selection for MRI

Constantino Carlos Reyes-Aldasoro and Abhir Bhalerao

Department of Computer Science, Warwick University, Coventry, UK.
{creyes,abhir}@dcs.warwick.ac.uk

Abstract. This paper considers the problem of classification of Magnetic Resonance Images using 2D and 3D texture measures. Joint statistics such as co-occurrence matrices are common for analysing texture in 2D since they are simple and effective to implement. However, the computational complexity can be prohibitive especially in 3D. In this work, we develop a texture classification strategy by a sub-band filtering technique that can be extended to 3D. We further propose a feature selection technique based on the Bhattacharyya distance measure that reduces the number of features required for the classification by selecting a set of *discriminant* features conditioned on a set training texture samples. We describe and illustrate the methodology by quantitatively analysing a series of images: 2D synthetic phantom, 2D natural textures, and MRI of human knees.
Keywords: Image Segmentation, Texture classification, Sub-band filtering, Feature selection, Co-occurrence.

1 Introduction

There has been extensive research in texture analysis in 2D and even if the concept of texture is intuitively obvious it can been difficult to give a satisfactory definition. Haralick [7] is a basic reference for statistical and structural approaches for texture description, contextual methods like Markov Random Fields are used by Cross and Jain [3], and fractal geometry methods by Keller [9]. The dependence of texture on resolution or scale has been recognised and exploited by workers in the past decade.

Texture description and analysis using a frequency approach is not as common as the spatial-domain method of co-occurrence [4] but there has been renewed interest in the use of filtering methods akin to Gabor decomposition [10] and joint spatial/spatial-frequency representations like Wavelet transforms [17]. Although easy to implement, co-occurrence measures are outperformed by such filtering techniques (see [13]) and have prohibitive costs when extended to 3D.

The importance of Texture in MRI has been the focus of some researchers, notably Lerksi [5] and Schad [16], and a COST European group has been established for this purpose [2]. Texture analysis has been used with mixed success in MRI, such as for detection of microcalcification in breast imaging [4] and for knee segmentation [8], and in Central Nervous System (CNS) imaging to detect

macroscopic lesions and microscopic abnormalities such as for quantifying contralateral differences in epilepsy subjects [15], to aid the automatic delineation of cerebellar volumes [12] and to characterise spinal cord pathology in Multiple Sclerosis [11]. Most of this reported work, however, has employed solely 2D measures, usually co-occurrence matrices that are limited by computational cost. Furthermore, feature selection is often performed in an empirical way with little regard to training data which are usually available.

Our contribution in this work is to implement a fully 3D texture description scheme using a multiresolution sub-band filtering (based on the Wilson and Spann [18] FPSS) and to develop a strategy for selecting the most *discriminant* texture features conditioned on a set of training images containing examples of the tissue types of interest (a 2D version of the method was presented in [14] without the 3D extension nor the feature selection). The ultimate goal is to select a compact and appropriate set of features thus reducing the computationally burden in both feature extraction and subsequent classification. We describe the 2D and 3D frequency domain texture feature representation and the feature selection method, by illustrating and quantitatively comparing results on 2D images and 3D MRI.

2 Materials and Methods

For this work three textured data sets were used:

1. **2D** Synthetic phantom of artificial textures; random noise and oriented patterns with different frequencies and orientation,
2. **2D** 16 natural textures from the Brodatz album arranged by Randen and Husøy [13]. This is a difficult image, the individual images have been histogram equalised, even to the human eye, some boundaries are not evident,
3. **3D** MRI of a human knee. The set is a sagittal T1 weighted with dimensions $512 \times 512 \times 87$, each pixel is 0.25 mm and the slice separation is 1.4 mm.

Figure 1 presents the data sets, in the case of the MRI only one slice (54) is shown. Throughout this work we will consider that an image, $\mathcal{I}$, has dimensions for rows and columns $N_r \times N_c$ and is quantised to N_g grey levels. Let $L_c = \{1, 2, \ldots, N_c\}$ and $L_r = \{1, 2, \ldots, N_r\}$ be the horizontal and vertical spatial domains of the image, and $G = \{1, 2, \ldots, N_g\}$ the set of grey tones. The image $\mathcal{I}$ can be represented then as a function that assigns a grey tone to each pair of coordinates:

$$L_r \times L_c; \mathcal{I} : L_r \times L_c \rightarrow G \tag{1}$$

2.1 Multiresolution Sub-band Filtering: The Second Orientation Pyramid (SOP)

Textures can vary in their spectral distribution in the frequency domain, and therefore a set of sub-band filters can help in their discrimination: if the image contains textures that vary in orientation and frequency, then certain filter sub-bands will be more energetic than others, and 'roughness' will be characterised by

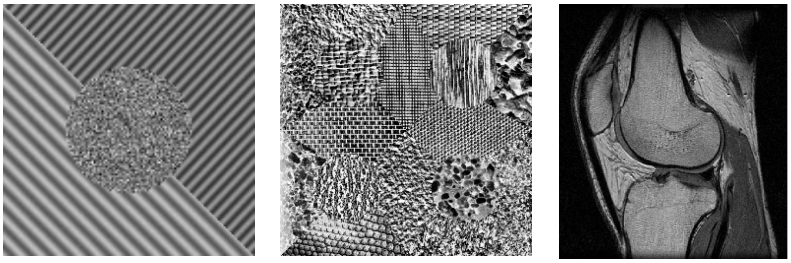

(a) (b) (c)

Fig. 1. Materials used for this work: three sets of images (a) Synthetic Phantom (2D), (b) Natural Textures (2D), (c) MRI of human knee (3D).

more or less energy in broadly circular band-pass regions. Wilson and Spann [18] proposed a set of operations that subdivide the frequency domain of an image into smaller regions by the use of compact and optimal (in spatial versus spatial-frequency energy) filter functions based on finite prolate spheroidal sequences (FPSS). The FPSS are real, band-limited functions which cover the Fourier half-plane. In our case we have approximated these functions with truncated Gaussians for an ease of implementation with satisfactory results (figure 3). These filter functions can be regarded as a band-limited Gabor basis which provides for frequency localisation.

Any given image $\mathcal{I}$ whose centred Fourier transform is $\mathcal{I}_\omega = \mathcal{F}\{\mathcal{I}\}$ can be subdivided into a set of regions $L_r^i \times L_c^i$: $L_r^i = \{r, r+1, \ldots, r+N_r^i\},\ 1 \leq r \leq N_r - N_r^i$, $L_c^i = \{c, c+1, \ldots, c+N_c^i\},\ 1 \leq c \leq N_c - N_c^i$, that follow the conditions: $L_r^i \subset L_r,\ L_c^i \subset L_c,\ \sum_i N_r^i = N_r,\ \sum_i N_c^i = N_c, (L_r^i \times L_c^i) \cap (L_r^j \times L_c^j) = \{\phi\}, i \neq j$.

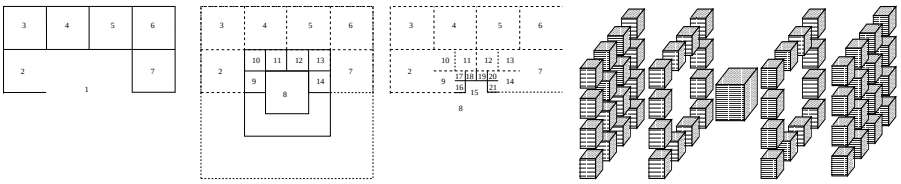

(a) (b) (c) (d)

Fig. 2. 2D and 3D Second Orientation Pyramid (SOP) tessellation. Solid lines indicate the filters added at the present order while dotted lines indicate filters added in lower orders. (a) 2D order 1, (b) 2D order 2, (c) 2D order 3, and (d) 3D order 1.

For this work, the Second Orientation Pyramid (SOP) tessellation presented in figure 2 was selected for the tessellation of the frequency domain. The SOP tessellation involves a set of 7 filters, one for the low-pass region and six for the

high-pass, and they are related to the i subdivisions of the frequency domain as:

$$L_r \times L_c; F^i : \begin{cases} L_r^i \times L_c^i & \to N(\mu^i, \Sigma^i) \\ (L_r^i \times L_c^i)^c & \to 0 \end{cases} \quad \forall i \in SOP \tag{2}$$

where μ^i is the centre of the region i and Σ^i is the variance of the Gaussian that will provide a cut-off of 0.5 at the limit of the band (figure 3).

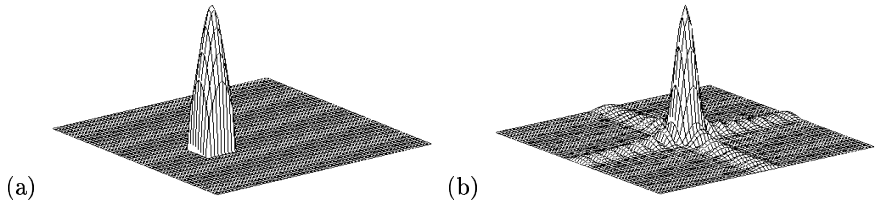

Fig. 3. Band-limited Gaussian Filter F^i (a) Frequency domain, (b) Spatial Domain.

The Feature Space S_ω^i in its frequency and spatial domains will be defined as:

$$S_w^i(k,l) = F^i(k,l) I_\omega(k,l) \;\; \forall (k,l) \in (L_r \times L_c), \qquad S^i = \mathcal{F}^{-1}\{S_\omega^i\} \tag{3}$$

Every order of the SOP Pyramid will consist of 7 filters. The same methodology for the first order can be extended to the next orders. At ever step, one of the filters will contain the low-pass (i.e. the centre) of the region analysed, $\mathcal{I}_\omega$ for the first order, and the six remaining will subdivide the high-pass bands or the surround of the region. This is detailed in the following co-ordinate systems: **Centre** : $F^1 : L_r^1 = \{\frac{N_r}{4} + 1 \ldots \frac{3N_r}{4}\}, L_c^1 = \{\frac{N_c}{4} + 1 \ldots \frac{3N_c}{4}\}$, **Surround** : $F^{2-7} : L_r^{3,4,5,6} = \{1 \ldots \frac{N_r}{4}\}, L_r^{2,7} = \{\frac{N_r}{4} + 1 \ldots \frac{N_r}{2}\}, L_c^{2,3} = \{1 \ldots \frac{N_c}{4}\}, L_c^4 = \{\frac{N_c}{4} + 1 \ldots \frac{N_c}{2}\}, L_c^5 = \{\frac{N_c}{2} + 1 \ldots \frac{3N_c}{4}\}, L_c^{6,7} = \{\frac{2N_c}{4} + 1 \ldots N_c\}$.

For a pyramid of order 2, the region to be subdivided will be the first central region described by $(L_r^1(1) \times L_c^1(1))$ which will become $(L_r(2) \times L_c(2))$ with dimensions $N_r(2) = \frac{N_r(1)}{2}, N_c(2) = \frac{N_c(1)}{2}$, (or in general $N_{r,c}(o+1) = \frac{N_{r,c}(o)}{2}$, for any order o). It is assumed that $N_r(1) = 2^a, N_c(1) = 2^b$ so that the results of the divisions are always integer values. The horizontal and vertical frequency domains are expressed by: $L_r(2) = \{\frac{N_r(1)}{4} + 1 \ldots \frac{3N_r(1)}{4}\}$, $L_c(2) = \{\frac{N_c(1)}{4} + 1 \ldots \frac{3N_c(1)}{4}\}$ and the next filters can be calculated recursively: $L_r^8(1) = L_r^1(2)$, $L_c^8(1) = L_c^1(2)$, $L_r^9(1) = L_r^2(2)$, etc.

Figure 4 shows the feature space S^i of the 2D synthetic phantom shown in figure 1(a). Figure 4(a) contains the features of orders 1 and 2, and figure 4(b) shows the features of orders 2 and 3. Note how in S^{2-7}, the features that are from high pass bands, only the central region, which is composed of noise, is present. The oriented patterns have been filtered out. S^{10} and S^{20} show the activation due to the oriented patterns. S^8 is a low pass filter and still keeps a trace of one of the oriented patterns.

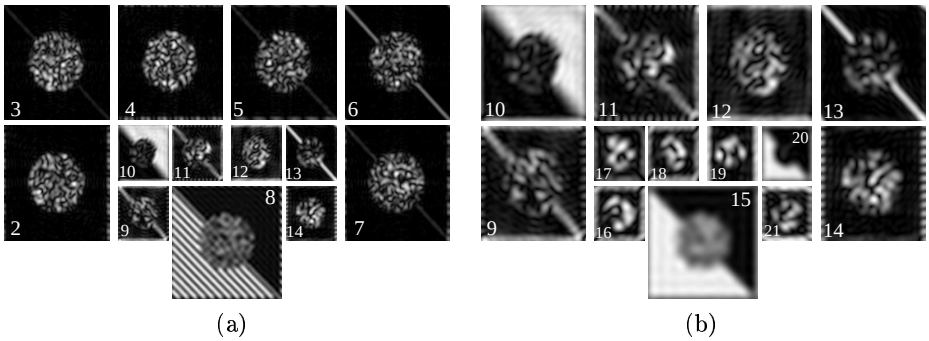

Fig. 4. Two sets of features S^i from the phantom image (a) Features 2 to 14 (Note S^{10} which describes one oriented pattern) (b) Features 9 to 21 (Note S^{20} which describes one oriented pattern). In each set, the feature S^i is placed in the position corresponding to the filter F^i in the frequency domain.

2.2 3D Multiresolution Sub-band Filtering

In order to filter a three dimensional set, a 3D tessellation (figure 2(d)) is required. The filters will again be formed by truncated 3D Gaussians in a octave-wise tessellation that resemble a regular oct-tree configuration. In the case of MR data, these filters can be applied directly to the K-space. As in the 2D case, the low pass region will be covered by one filter, and for the high pass there are 28 filters. This tessellation yields 29 features per order. As in the two dimensional case, half of the space is not used because of the symmetric properties of the Fourier transform. The definitions of the filters follows the extension of the space of rows and columns to $L_r \times L_c \times L_l$ with the new dimension l - levels.

2.3 Discriminant Feature Selection: Bhattacharyya Space and Order statistics

Feature selection is a critical step in classification since not all features derived from sub-band filtering, co-occurrence matrix, wavelets, wavelet packet or any other methodology have the same discrimination power. In many cases, a large number of features are included into classifiers or reduced by principal components analysis (PCA) or other methods without considering that some of those features will not help to improve classification but will consume computational efforts. As well as making each feature linearly independent, PCA allows the ranking of features according to the size of the global covariance in each principal axis from which a 'subspace' of features can be presented to a classifier. Fisher linear discriminant analysis (LDA) diagonalises the features space constrained by maximising the ratio between-class to within-class variance and can be used together with PCA to rank the features by their 'spread' and select a discriminant subspace [6]. However, while these eigenspace methods are optimal and effective, they still require the computation of all the features for given data.

We propose a feature selection methodology based on the discrimination power of the individual features taken independently, the ultimate goal is select a reduced number m of features or bands (in the 2D case $m \leq 7o$, and in 3D $m \leq 29o$, where o is the order of the SOP tessellation). It is sub-optimal in the sense that there is no guarantee that the selected feature sub-space is the best, but our method does not exclude the use of PCA or LDA to diagonalise the result to aid the classification.

A set of *training* classes are required, which make this a supervised method. Four training classes of the human knee MRI have been manually segmented and each class has been sub-band filtered in 3D. Figure 5 shows the scatter plot of three *bad* and three *good* features arbitrarily chosen.

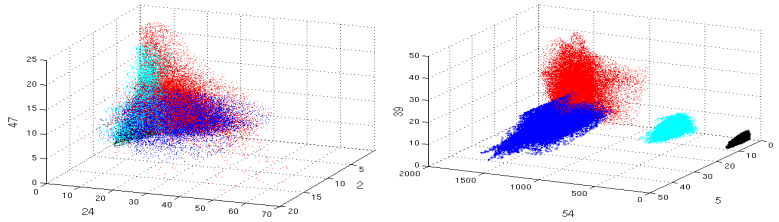

(a) (b)

Fig. 5. Scatter plots of three features S^i from human knee MRI (3D, order 2) (a) *bad* discriminating features $S^{2,24,47}$ (b) *good* discriminating features $S^{5,39,54}$. Note that each feature corresponds to a filtered version of the data, therefore the axis values correspond to the grey levels of each feature.

In order to obtain a quantitative measure of *how separable* two classes are, a distance measure is required. We have studied a number measures (Bhattacharyya, Euclidean, Kullback-Leibler, Fisher [1]) and concluded that the *Bhattacharyya distance* [6] is the most convenient. The variance and mean of each class are computed to calculate a distance in the following way:

$$B(a,b) = \frac{1}{4}\ln\left\{\frac{1}{4}\left(\frac{\sigma_a^2}{\sigma_b^2} + \frac{\sigma_b^2}{\sigma_a^2} + 2\right)\right\} + \frac{1}{4}\left\{\frac{(\mu_a - \mu_b)^2}{\sigma_a^2 + \sigma_b^2}\right\} \tag{4}$$

where: $B(a,b)$ is the Bhattacharyya distance between $a-th$ and $b-th$ classes, σ_a is the variance of the $a-th$ class, μ_a is the mean of the $a-th$ class, and a, b are two different training classes.

The Mahalanobis distance used in Fisher LDA is a particular case of the Bhattacharyya, when the variances of the two classes are equal, this would eliminate the first term of the distance. The second term, on the other hand will be zero if the means are equal and is inversely proportional to the variances. $B(a,b)$ was calculated for the four training classes (background, muscle, bone and tissue) of the human knee MRI (figure 1(c)) with the following results:

	μ	σ	Background	Muscle	Bone	Tissue
Background	91	49	0	4.36	12.51	11.70
Muscle	696	140	4.36	0	3.25	3.26
Bone	1605	212	12.51	3.25	0	0.0064
Tissue	1650	227	11.70	3.26	0.0064	0

It should be noted the small Bhattacharyya distance between the tissue and the bone classes. These two classes have low discrimination power.

For n classes with S^i features, each class pairs (p) at feature i will have a Bhattacharyya distance $B^i(a,b)$, and that will produce a Bhattacharyya Space of dimensions $N_p = \binom{n}{2}$ and $N_i = 7o$: $N_p \times N_i$. The domains are $L_i = \{1, 2, \ldots 7o\}$ and $L_p = \{(1,2), (1,3), \ldots (a,b), \ldots (n-1,n)\}$ where o is the order of the pyramid. The Bhattacharyya Space, BS, is defined then as:

$$L_p \times L_i; BS : L_p \times L_i \rightarrow B^i(S_a^i, S_b^i) \tag{5}$$

whose marginal $BS^i = \sum_{p=1}^{N_p} B^i(S_a^i, S_b^i)$ is of particular interest since it sums the Bhattacharyya distance of every pair of a certain feature and thus will indicate how discriminant a certain filter is over the whole combination of class pairs. Figure 6(a) Shows the Bhattacharyya Space for the 2D image of Natural Textures shown in figure 1(b), and figure 6(b) shows the marginal BS^i.

The selection process of the most discriminant features that we propose uses the marginal of the Bhattacharyya space BS^i that indicates which filtered feature is the most discriminant. The marginal is a set

$$BS^i = \{BS^1, BS^2, \ldots BS^{7o}\}, \tag{6}$$

which can be sorted in a decreasing order, its order statistic will be:

$$BS^{(i)} = \{BS^{(1)}, BS^{(2)}, \ldots BS^{(7o)}\}, \quad BS^{(1)} \geq BS^{(2)} \geq \ldots \geq BS^{(7o)}. \tag{7}$$

This new set can be used in two different ways, first, it provides a particular order in which the feature space can be fed into a classifier, and with a mask provided, the error rate can be measured to see the contribution of each feature into the final classification of the data. Second, it can provide a *reduced set* or sub-space; a group of training classes of reduced dimensions can show which filters are adequate for discrimination and thus use only those filters.

3 Classification of the feature space

For every data set the feature space was classified with a K-means classifier, which was selected for simplicity and speed. The feature space was introduced to the classifier by the order statistic $BS^{(i)}$, one at the time (that is, the feature and the mean from the training data; $k = 1, 2, 3, \ldots$) and for each additional feature included, the misclassification error was calculated. Figures 9 (c) and 10 (c) show the misclassification as the features are included and k increased.

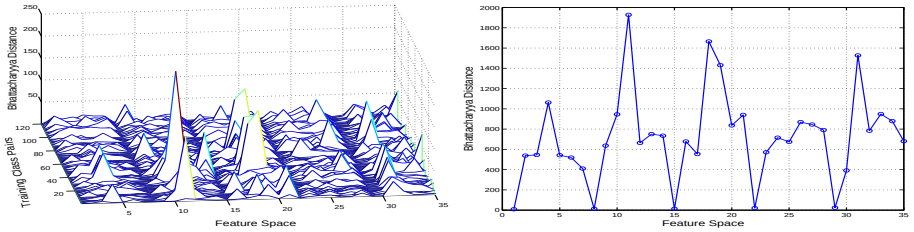

(a) (b)

Fig. 6. Natural textures (a) Bhattacharyya Space BS (2D, order 5 = 35 features), $(\binom{16}{2} = 120\ pairs)$, (b) Corresponding marginal of the Bhattacharyya Space BS^i.

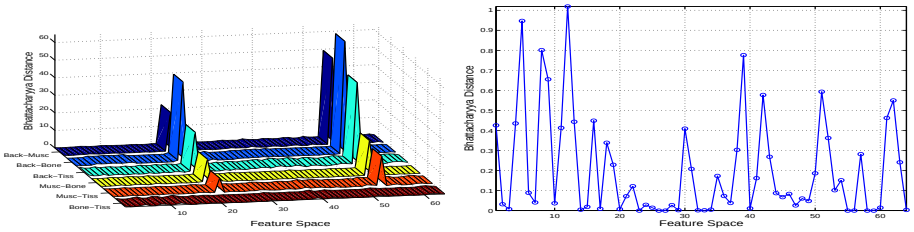

(a) (b)

Fig. 7. Human knee MRI (a) Bhattacharyya Space BS (3D, order 2) $\binom{3}{4} = 6\ pairs$ (b) Bhattacharyya Space($BS^i(bone, tissue)$).

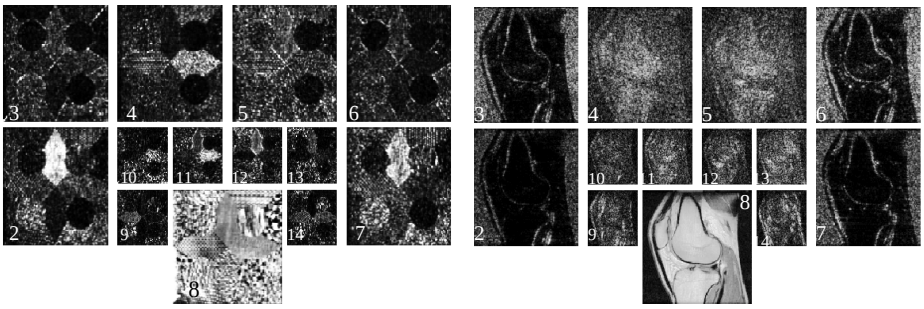

(a) (b)

Fig. 8. Two sets of features S^i from different images: (a) Features 2 to 14 of the Natural Textures image (b) Features 2 to 14 from one slice of the human knee MRI.

Figures 4 and 8 show the features spaces S^i of the sub-band filtering process (for the MRI only one slice, 54 is shown). For the synthetic phantom two features $S^{10,20}$ highlight the oriented patterns. For the natural textures the S^i is more complexbut still some of the textures are highlighted in certain features. For instance, $S^{2,7}$ highlight one of the upper central textures that is of high frequency. Note also that the S^{3-6}, the upper row have a low value for the circular regions, i.e. they have been filtered since their nature is of lower frequencies.

For the human knee S^i the first observation is the high pass nature of the background in $S^{2,3,6,7}$, which could be expected for the noise nature of the background, but $S^{4,5}$, do not describe the background but rather the bone of the knee. S^8 is a low pass filtered version of the original slice.

The Bhattacharyya Spaces in figures 6, 7 present very interesting information towards the selection of the features for classification. In the natural textures case, a certain periodicity can be found; the $BS^{1,7,14,21,28}$ have the lowest values. This implies that the low-pass features provide no discrimination at all.

The human knee MRI Bhattacharyya Space (Figure 7)(a) was formed with four $32 \times 32 \times 32$ training regions of background, muscle, bone. These training regions, which are small relative to the size of the data set, were manually segmented, and they will remain as part of the data to classify. It can be immediately noticed that two bands ($S^{22,54}$, low-pass) dominate the discrimination while the distance of the pair *bone-tissue* is practically zero compared with the rest of the space. If the marginal were calculated like in the previous cases, the low-pass would dominate and the discrimination of the bone and tissue classes, which are difficult to segment would be lost. Figure 7 (b) zooms into the Bhattacharyya space of this pair. Here we can see that some features: 12, 5, 8, 38, ..., could provide discrimination between bone and tissue, and the low pass bands could help discriminate the rest of the classes.

4 Discussion

Figure 9 (a) shows the classification of the 2D synthetic phantom at 4.3% misclassification with 7 features (out of 35). Of particular importance were features 10 and 20 which can be seen in the marginal of the Bhattacharyya space in figure 9 (b). The low-pass features 1 and 8 also have high values but should not be included in this case since they contain the frequency energy that will be disclosed in features 10 and 20 giving more discrimination power.

The misclassification plot in figure 9 (c) shows how the first two features manage to classify correctly more than 90% of the pixels and then the next 5, which describe the central circular region, decrease the misclassification. If more features are added, the classification would not improve.

The natural textures image present a more difficult challenge. Randen and Husøy [13] used 9 techniques to classify this image, interestingly, they did not used FPSS filtering. Some of their misclassification results were Dyadic Gabor filter banks (60.1%), Gabor filters (54.8%), co-occurrence (49.6%), Laws filters (48.3%), Wavelets (38.2%), quadrature mirror filters (36.4%). The misclassification of SOP filtering is 37.2%, placing this in second place. Figure 10(a) shows

the final classification and figure 10(b) show the pixels that were correctly classified. The misclassification decreases while adding features and requires almost all of them in contrast with the synthetic phantom previously described.

The most important figure of the materials is the Human knee MRI. The original data set consisted of 87 slices of 512×512 pixels each. The classification was performed with the low-pass feature, 54, and the ordered statistics of the bone-tissue feature space: $S^{12,5,8,39,9,51,42,62}$. This reduced significantly the computational burden since only these features were filtered. The misclassification obtained was 8.1%. Several slices in axial, coronal and sagittal planes with their respective classifications are presented in figure 11.

To compare the discrimination power of the sub-band filtering technique with the co-occurrence matrix, one slice of the human knee MRI set was selected and classified with both methods. The major disadvantage of the co-occurrence matrix is that its dimensions will depend on the number of grey levels. In many cases, the grey levels are quantised to reduce the computational cost and information is lost inevitably. Otherwise, the computational burden just to obtain the original matrix is huge.

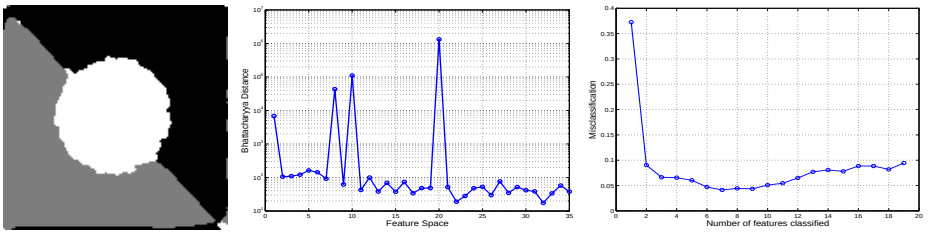

(a) (b) (c)

Fig. 9. Classification of the figure 1(a), (a) Classified 2D Phantom at misclassification 4.13% (b) Marginal Distribution of the Bhattacharyya Space BS^i. (Note the high values for features 10 and 20) (c) Misclassification per features included.

The Bhattacharyya Space was calculated with the same methodology and the 10 most discriminant features were Contrast: $f_2(\theta = 0, \frac{\pi}{2}, \frac{3\pi}{4})$, Inverse difference moment: $f_5(\theta = \frac{3\pi}{4})$, Variance $f_{10}(\theta = 0, \frac{\pi}{2}, \frac{3\pi}{4})$, Entropy $f_{11}(\theta = 0, \frac{\pi}{2}, \frac{3\pi}{4})$. The misclassification obtained with these 10 features was 40.5%. To improve the classification, the gray-level original data was included as another feature and in this case, with the first 6 features the misclassification reached 17.0%. With the SOP, this slice had a misclassification of 7%.

5 Conclusions

Three data sets were classified with our methodology. The first was a simple combination of artificial textures mainly for visualisation purposes. The second

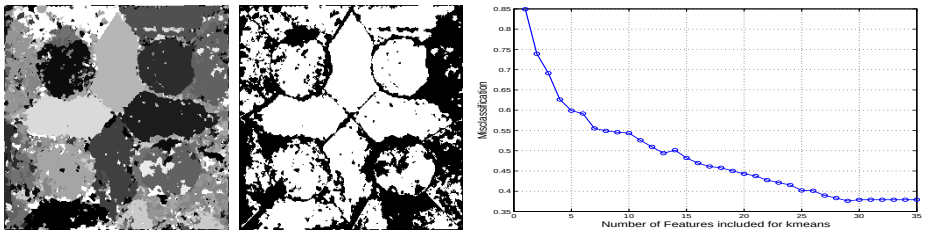

(a) (b) (c)

Fig. 10. Classification of the natural textures image (figure 1(b)) with 16 different textures (a) Classification results at 37.2% misclassification (b) Pixels correctly classified,(c) misclassification error for the sequential inclusion of features to the classifier.

a combination of natural textures which are quite difficult to segment, these were included to show the power of the method. The third and most interesting was a 3D MRI set of a Human Knee, which was successfully segmented.

The Second Orientation Pyramid Sub-Band Filtering is a powerful and simple technique to discriminate both natural and synthetic textures and extends well to 3D. The number of features can be drastically reduced by feature selection through the Bhattacharyya Space to a most discriminant subset, either from the marginal or an individual class pair distances. This feature selection technique can be applied with similar classification schemes like wavelets or co-occurrence where a number of features are to be discarded before classifying. Our results compared with the co-occurrence matrix and show the misclassification for the sub-band filtering is almost half for the MRI, and as good as Randen's [13] for the natural textures. While co-occurrence is not easily extended to three dimensions, we can employ our feature selection method for effectively selecting a compact set of discriminant features for this scheme. This method could be linked to contextual classification methods that can improve the misclassification rates.

References

1. A. Bhalerao and N. Rajpoot. Selecting Discriminant Subbands for Texture Classification. In *submitted to BMVC'03*, 2003.
2. COST European Cooperation in the field of Scientific and Technical Research. *COST B11 Quantitation of MRI Texture*. http://www.uib.no/costb11/, 2002.
3. G. R. Cross and A. K. Jain. Markov Random Field Texture Models. *IEEE Trans. on PAMI*, PAMI-5(1):25–39, 1983.
4. D. James et al. Texture Detection of Simulated Microcalcification Suceptibility Effects in MRI of the Breasts. *J. Mag. Res. Imaging*, 13:876–881, 2002.
5. R.A. Lerski et.al. MR Image Texture Analysis - An Approach to Tissue Characterization. *Mag. Res. Imaging*, 11(6):873–887, 1993.
6. K. Fukanaga. *Introd. to Statistical Pattern Recognition*. Academic Press, 1972.
7. R. M. Haralick. Statistical and Structural Approaches to Texture. *Proceedings of the IEEE*, 67(5):786–804, 1979.

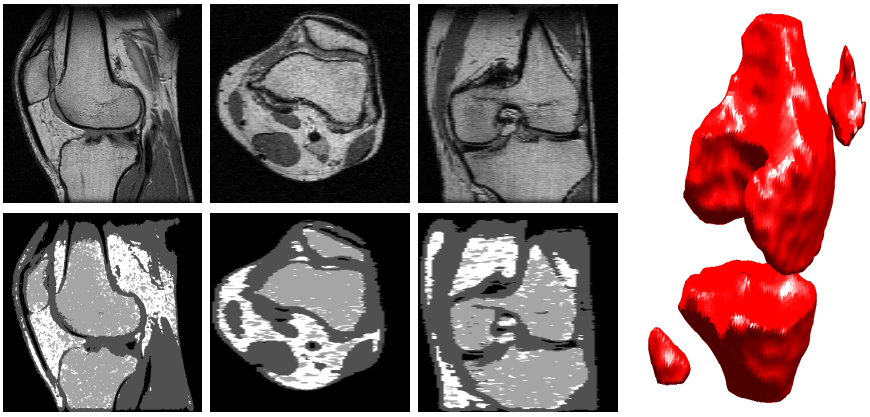

Fig. 11. Human knee MRI and their classification (misclassification 8.1%)(a) Sagittal slice 45 (b) Axial slice 200 (c) Coronal slice 250 and (d) Rendering of the bone.

8. T. Kapur. *Model based three dimensional Medical Image Segmentation.* PhD thesis, AI Lab, Massachusetts Institute of Technology, May 1999.
9. J. M. Keller and S. Chen. Texture Description and Segmentation through Fractal Geometry. *Computer Vision, Graphics and Image Processing*, 45:150–166, 1989.
10. M. Eden M. Unser. Multiresolution Feature Extraction and Selection for Texture Segmentation. *IEEE Trans. on PAMI*, 11(7):717–728, 1989.
11. J. M. Mathias, P. S. Tofts, and N. A. Losseff. Texture Analysis of Spinal Cord Pathology in Multiple Sclerosis. *Mag. Res. in Medicine*, 42:929–935, 1999.
12. I. J. Namer O. Yu, Y. Mauss and J. Chambron. Existence of contralateral abnormalities revealed by texture analysis in unilateral intractable hippocampal epilepsy. *Magnetic Resonance Imaging*, 19:1305–1310, 2001.
13. T. Randen and J. Håkon Husøy. Filtering for Texture Classification: A Comparative Study. *IEEE Trans. on PAMI*, 21(4):291–310, 1999.
14. CC Reyes-Aldasoro and A Bhalerao. Sub-band filtering for mr texture segmentation. In *Proceedings of Medical Image Understanding and Analysis*, pages 185–188, Portsmouth, UK, July 2002.
15. N. Saeed and B. K. Piri. Cerebellum Segmentation Employing Texture Properties and Knowledge based Image Processing : Applied to Normal Adult Controls and Patients. *Magnetic Resonance Imaging*, 20:425–429, 2002.
16. L R Schad, S Bluml, and I Zuna. MR Tissue Characterization of Intracrianal Tumors by means of Texture Analysis. *Mag. Res. Imaging*, 11:889–896, 1993.
17. M. Unser. Texture Classification and Segmentation Using Wavelet Frames. *IEEE Trans. on Image Processing*, 4(11):1549–1560, 1995.
18. R. Wilson and M. Spann. Finite Prolate Spheroidal Sequences and Their Applications. *IEEE Trans. on PAMI*, 10(2):193–203, 1988.